

# UC Irvine

## UC Irvine Previously Published Works

### Title

Nanoelectronic three-dimensional (3D) nanotip sensing array for real-time, sensitive, label-free sequence specific detection of nucleic acids

### Permalink

<https://escholarship.org/uc/item/1qd3n750>

### Journal

Biomedical Microdevices, 18(1)

### ISSN

1387-2176

### Authors

Esfandyarpour, Rahim  
Yang, Lu  
koochak, Zahra  
[et al.](#)

### Publication Date

2016-02-01

### DOI

10.1007/s10544-016-0032-8

Peer reviewed



Published in final edited form as:

*Biomed Microdevices*. 2016 February ; 18(1): 7. doi:10.1007/s10544-016-0032-8.

## Nanoelectronic three-dimensional (3D) nanotip sensing array for real-time, sensitive, label-free sequence specific detection of nucleic acids

Rahim Esfandyarpour<sup>2</sup>, Lu Yang<sup>3</sup>, Zahra koochak<sup>1,2</sup>, James S. Harris<sup>1</sup>, and Ronald W. Davis<sup>2</sup>

Rahim Esfandyarpour: rahimes@stanford.edu

<sup>1</sup>Department of Electrical Engineering, Stanford University, Stanford, CA, USA

<sup>2</sup>Stanford Genome Technology Center, 3165 Porter Dr., Palo Alto, CA 94304, USA

<sup>3</sup>Department of Bioengineering, Stanford University, Stanford, CA, USA

### Abstract

The improvements in our ability to sequence and genotype DNA have opened up numerous avenues in the understanding of human biology and medicine with various applications, especially in medical diagnostics. But the realization of a label free, real time, high-throughput and low cost biosensing platforms to detect molecular interactions with a high level of sensitivity has been yet stunted due to two factors: one, slow binding kinetics caused by the lack of probe molecules on the sensors and two, limited mass transport due to the planar structure (two-dimensional) of the current biosensors. Here we present a novel three-dimensional (3D), highly sensitive, real-time, inexpensive and label-free nanotip array as a rapid and direct platform to sequence-specific DNA screening. Our nanotip sensors are designed to have a nano sized thin film as their sensing area (~20 nm), sandwiched between two sensing electrodes. The tip is then conjugated to a DNA oligonucleotide complementary to the sequence of interest, which is electrochemically detected in real-time via impedance changes upon the formation of a double-stranded helix at the sensor interface. This 3D configuration is specifically designed to improve the biomolecular hit rate and the detection speed. We demonstrate that our nanotip array effectively detects oligonucleotides in a sequence-specific and highly sensitive manner, yielding concentration-dependent impedance change measurements with a target concentration as low as 10 pM and discrimination against even a single mismatch. Notably, our nanotip sensors achieve this accurate, sensitive detection without relying on signal indicators or enhancing molecules like fluorophores. It can also easily be scaled for highly multiplexed detection with up to 5000 sensors/square centimeter, and integrated into microfluidic devices. The versatile, rapid, and sensitive performance of the nanotip array makes it an excellent candidate for point-of-care diagnostics, and high-throughput DNA analysis applications.

## Keywords

Nanotips array; Nanoelectric biosensor; Label-free; Single point mutations; DNA sequencing; Nanofabrication

---

## 1 Introduction

The improvements in our ability to sequence and genotype DNA have opened up numerous avenues in the understanding of human biology and medicine with various applications, especially in medical diagnostics. Single nucleotide polymorphisms, DNA sequence variations that occur every 50–100 base pairs when a single nucleotide in the genome differs between individuals of the same species or between paired chromosomes in an individual, can have significant effects on biological functions and have been associated with the development of several genetic diseases such as cystic fibrosis (Drumm et al. 2005) and Alzheimer's disease (Roses and Allen 1996). An inexpensive, simple, rapid, and sensitive method for the detection of single nucleotide polymorphisms (single point mutations) would accelerate research and facilitate clinical applications of genotyping. Many techniques and DNA biosensor technologies have been developed with their own advantages and disadvantages, but for these techniques speed is difficult to achieve except at the expense of accuracy. Traditional genotyping techniques include Sanger sequencing, which requires a DNA polymerase enzyme to incorporate chain-terminating dideoxynucleotides during DNA replication (Sanger et al. 1977; Sanger 1978); automated chain-termination DNA sequencing machines, which utilize four fluorescent dyes to label nucleotides and are highly dependent on resolution and efficient collection of the emission signals (Metzker 2005; Ansorge et al. 1987; Smith et al. 1986; Metzker et al. 1996; McBride et al. 1989); and pyrosequencing methods, which detects release of pyrophosphate during nucleotide incorporation rather than chain termination (Metzker et al. 1996; McBride et al. 1989; Ahmadian 2000; Huse 2007; Ronaghi 2001; Quince 2009a; Ronaghi et al. 1998; Adams et al. 1991; Ronaghi 1996). These techniques are expensive and largely rely on polymerase chain reaction (PCR) or comparable DNA amplification systems, which require additional time and reduce accuracy (Velculescu et al. 1995; Quince 2009b). In recent years, various DNA biosensor technologies are being developed using silicon electronic devices as an alternative to traditional methods, which are advantageous not only for their low cost, simplicity and sensitivity, but also for their amenability to miniaturization. Recent developments in nanotechnology have provided the necessary tools for the miniaturization of sensing and transducing platforms so that complicated electronic circuits can be integrated into a miniature device. Such inexpensive designs capable of accurately processing small sample volumes are necessary for point-of-care applications. Several electrochemical genosensors have been reported that have nanomolar-range sensitivity, but all to date rely on labeling techniques (Kannan 2011; Hashemi Rafsanjani et al. 2010). Labeling is an expensive, time-consuming, and labor-intensive procedure that introduces additional uncertain sources of error to the measurements (Esfandyarpour et al. 2013; Kricka 2002). Silicon Nanowires (SiNWs), one of the more sensitive and selective technologies for the detection of DNA hybridization, is quite limited in throughput (Park et al. 2002; Li et al. 2004; Li et al. 2005; Xie 2012; Cui et al. 2001; Zhang et al. 2008; Gao 2007). Electronic biosensors based on field-effect transistor

(FET) arrays suffer from the negative impact of the intrinsic drift characteristics of FET devices in electrolyte solutions on the performance of FET-based devices, and can only detect short DNA samples, which is not suitable for single nucleotide polymorphisms detection. In addition, the readout of binding events with this method is slow compared to the hybridization reaction [27–31]. Most of the other recent biosensors that allow electrical detection of DNA sequence with extreme sensitivity and excellent selectivity employ peptide nucleic acid (PNA) as the capture probe instead of DNA (Wang 1996; Zhang and Apella 2010). The typical length limit of PNA is approximately 20, which considerably confines its applications in diagnostic platforms, especially for detecting long DNA sequences (Zhang and Apella 2010). Therefore, there remains a lack of rapid, inexpensive, high throughput, real-time, and label-free methods, which display sensitivity and at the same time require a simpler and less time consuming protocol. In this study, we developed a 3D electrical nanotip array for sequence-specific DNA screening that meets these criteria (Fig. 1a).

## 2 Materials and methods

### 2.1 Nanotip sensors advantages, configuration and fabrication

The key criteria assessment for biosensors is the minimum detectable concentration of bio-species in an injected medium. This detection limit depends on several different factors such as sensitivity (the minimum number of similar binding events to occur to get a detectable signal, diffusion time of target molecules, flow rate, and sensor geometry. Designing nanotip sensors we improved this feature by designing the sensitive region of the sensor to be a thickness controllable thin film layer (~ 20 nm), sandwiched between two measuring electrodes. Only a few binding events in the nano-size sensing area of nanotip sensors are enough for impedance modulation and observation of a change in measured impedance across the sensing electrodes. We also designed our nanotip sensors to have a suspended three-dimensional (3D) geometry to assure that diffusion takes place in three dimensions in a channel. It results in a higher hit rate of target molecules to the probe molecule per sensor, and thus a faster detection platform, differing from current electrical biosensors that have planar (two-dimensional) structures. Another important design consideration of developed nanotip sensors is the array processing and multiplexing feature of this platform. Using highly developed standard optical lithography process; we successfully fabricated an array of nanotip sensors, with the sensor density of 2500 sensors/cm<sup>2</sup>, which makes it a suitable platform for high throughput genomics on a large scale.

The 3D nanotip sensors structure consists of four thin-film layers as shown in Fig. 1a. There are two conductive layers (100 nm) with an insulator layer sandwiched between them (20 nm). There are additional oxide layers that act as protective layers above and below the sensors. The top oxide layer (30 nm) prevents the exposure of the conductive electrodes to the solution. Underneath the protective oxide layer (200 nm) is a thermally grown oxide, which is the thickest layer of nanotip sensors and insulates the bottom electrodes from the substrate. The nano-size middle oxide layer enables detection and is the key element to make these 3D devices highly sensitive. As explained above, any small change in the population of molecules at the surface of the nano-size tip results in a change in measured impedance across the sensing electrodes. We successfully fabricated an array of nanotip

sensors on a four-inch silicon wafer using the standard photolithography process followed by several depositions and etching steps (Fig. 1c). The fabrication process starts with thermally growing 200 nm of SiO<sub>2</sub> in a high temperature atmospheric furnace on a silicon wafer (100) to insulate the substrate from the other layers. This furnace is made of pure quartz that allows for the introduction and mixing of gases (N<sub>2</sub>, Ar, O<sub>2</sub> and H<sub>2</sub>) to easily grow silicon dioxide (SiO<sub>2</sub>) layers. The bottom 200 nm SiO<sub>2</sub> layer with the crystal orientation of 100 at the temperature of 1100 °C was grown in about 2 h. Then the bottom conductive electrodes of the nanotip sensors were patterned through an optical lithography process followed by metal deposition and a lift off process. After pre-baking of the wafer on a hot plate at 200 °C for two hours, 10 drops of Hexamethyldisilazane (HMDS) were applied, on top of which MaP 1215 resist was applied. After performing near-UV photoresist exposure for 3 s, the exposed resist was developed in MaD 331 for 35 s followed by immediately rinsing in water. The patterned wafer then was transferred to an evaporation system to deposit 3 nm of Cr as an adhesive layer, and 100 nm of gold as the bottom conductive electrodes. After the lift off process in acetone for 30 min and rinsing in water, 20 nm of silicon dioxide (nano size sensitive region) was deposited using a plasma-assisted atomic layer deposition (ALD) technique. This sensitive middle oxide nanolayer was deposited as a high quality, conformal, uniform, pinhole and particle free oxide film using BTBAS as the precursor and Argon (Ar) as the purging gas, while the deposition temperature was 300 °C. The fabrication process was followed by deposition of the top conductive electrodes following the same procedure as the bottom conductive electrodes. The protective oxide layer was then deposited using a low temperature (350 °C) plasma-enhanced chemical vapor deposition (PECVD) system, followed by several etching and optical lithography steps to form the channels underneath the fabricated nanotip sensors. After removing the oxide layer from the measuring pads through a wet etching process (using 6:1 Buffered Oxide Etch) and exposing the bonding pads for wire binding, sharp edges of the nanotip sensors in the channel were formed through a physical etching mechanism, focused ion beam (FIB). Finally a microfluidic PDMS channel was thermally bonded on top of the fabricated array (Fig. 1b) to enable sensing experiments using microfluidic flow.

## 2.2 Materials

Probe DNA, 45 base pairs long, with biotinylated modification at 5' end and sequence of 5' – ACACCTGCACTACCACACTCCCTCACACTGACAAATGATCACCCC-3', and the target DNA complementary to the probe DNA and with a sequence of 5' - AGGTGTGGGGTGATCATTGTCAGTGTGAGGGAGTGTGGTAGTGC-3', were both purchased from Life Technologies. We also used non-target DNA with a single mismatch at the 27th position, with a sequence of “AGGTGTGGGGTGATCATTGTCAGTGTGCGAGGGAGTGTGGTAGTGC” and non-complimentary DNA with a biotinylated label at the 5' end and a sequence of “CTTGTGTTTGTGTCGACGGGTGACTCACACTTTCTGTGTTGCTGTA”. Streptavidin (S4762), Bovine Serum Albumin (A9418), and Biotin Labeled Bovine Albumin (A8549) used for these experiments were purchased from Sigma-Aldrich. 10X PBS buffer stock was used for solution preparation.

### 2.3 Surface modification for primary amines

Biotinylated Bovine Serum Albumin (BBSA) with a concentration of 1 mg/ml diluted in 1X PBS was injected into the channel to physically be immobilized on the sensor tip. After waiting for 30 min to ensure maximal coverage and immobilized of BBSA molecules on the sensor tip, 20  $\mu$ l of 1 mg/ml streptavidin was incubated in the channel for 20 min in order to bind the biotinylated BSA. Next, 20  $\mu$ l of probe DNA sequence (45 base pairs long), which is biotinylated at the 5' end, with a concentration of 10  $\mu$ M was incubated in the channel to be captured by the streptavidin molecules immobilized on the sensors' tip. 20 min incubation time was necessary to produce optimal immobilization results. Finally, 20  $\mu$ l of 1 mg/ml Bovine Serum Albumin (BSA) was injected into the microfluidic channel and incubated for 10 min to prevent any nonspecific binding (Fig. 2). These primary DNA-functionalized nanotip sensors were used for further experiments.

### 2.4 Electrochemical impedance spectroscopy detection

In order to perform Electrochemical Impedance Spectroscopy (EIS) using the nanotip sensors, a Versa STAT3 potentiostat (Princeton Instruments, Princeton, New Jersey) was used. A sinusoidal voltage signal was applied to the top electrodes and the current entering the bottom electrode was measured and used to calculate the modulated impedance. According to our experiments, the optimal frequency at which maximum change in measured impedance occurs due to biomolecular binding is between 1 and 100 kHz. Thus we chose 15 kHz as the operating frequency (250 mV RMS AC signal) for all measurements with the sampling rate of one sample every 4 s. All measurements were performed at room temperature (23  $^{\circ}$ C). Used microfluidic channels dimensions were 300  $\mu$ m-wide and 80  $\mu$ m-height, which were made of poly (dimethylsiloxane) (PDMS) patterned by pre-made SU8 mold and thermally bound onto the sensors and fixed on a wafer for further experiments.

## 3 Results and discussion

### 3.1 Label-free detection of specific single-stranded DNA molecules and single point mutations

In order to demonstrate the utility of developed nanotip sensors for label free and real time detection of specific single-stranded DNA molecules (45 base pairs) and single point mutations (at 27th position), EIS and impedance spectrum monitoring were performed. EIS is very sensitive to changes in interfacial impedance upon bio-recognition events occurring at the surface-electrolyte interface. For all the experiments, before running the measurements, the microfluidic channel was washed with a wash buffer for 30 min with the flow rate of 5  $\mu$ l/min to wash off all primary DNA molecules not captured by the functionalized BBSA-Streptavidin layer at the sensor tip. The impedance level of each primary amine-coated sensor was measured in real time while the wash buffer was in the microfluidic channel. Afterward, the test sample containing the complementary single-stranded target DNA was injected into the channel and incubated for 30 min. This was enough time for the target DNA to hybridize to immobilized probe oligonucleotides on the sensor tip and form a double helix. Nonspecific binding of species gently washed away using wash buffer and the impedance level was measured. As shown in Fig. 3, real time measured impedance, a clear change in impedance after hybridization of the complementary

single stranded target DNA to the probes DNA was observed. As explained in detail in the modeling section, the change in measured impedance was due to the formation of the double-stranded helix at the sensor interface, which results in a change in relative dielectric permittivity at the sensitive region of nanotip sensors. Consequently, relative dielectric permittivity change results an increase in capacitance and thus a decrease in measured impedance. Frequency spectra of the nanotip sensors, Bode plots, before and after formation of double helix of DNA molecules (hybridization event) are also shown in Fig. 5c. These spectra demonstrate the ability of the nanotip sensors to measure impedance differences across a range of frequencies from 1 to 25KHz.

### 3.2 Model study

To fully understand the nanotip sensors' behavior and the mechanisms affecting the measured results, we modeled and characterized the interface of the nanotip sensors with the electrolyte as well as the circuit model of the sensor. According to the full-developed circuit model of the nanotip sensors, shown in Fig. 5b, there are several parasitic impedance components at the sensor interface. Parasitic components containing fringing capacitance ( $C_f$ ), parasitic resistance across the double layer at the interface of nanotip sensors between the electrodes ( $R_f$ ), double layer capacitance on each conductive electrode surface ( $C_{dl}$ ), parasitic tunneling resistance or the electron transfer resistance from the electrodes into the bulk solution ( $R_t$ ) and the bulk resistance of the electrolyte ( $R_s$ ). In order to understand the sensor behavior we need to understand the physics of each parasitic component at the nanotip sensors interface and the formation mechanisms behind them. We begin with the double layer capacitance ( $C_{dl}$ ), resulting from accumulation of ions, which consists of two nanolayers. One layer is an adsorbed fixed layer of the ions, called the stern layer, which is a concentration-independent layer and estimated to be roughly 1 nm from the sensor surface. The second nanolayer, called the diffuse layer, is another ion-accumulating layer to satisfy the condition of charge neutrality and neutralize the charge in the stern layer. The double layer capacitance is the result of both of the above layers that can be represented by two capacitors in series,  $C_{ad}$  and  $C_{diff}$ .

$$\frac{1}{C_{dl}} = \frac{1}{C_{ad}} + \frac{1}{C_{diff}}$$

One of these two capacitances is normally dominant depending on the medium's salt concentration. Considering the salt concentration of the buffer used in our study, we estimate the diffuse layer thickness to be about 10 nm (Zhang and Apella 2010) and the double layer capacitance is dominated by stern layer capacitance. Knowing this, we can estimate the impedance value of the double layer capacitance at 15kHz, which will be  $\sim 1 \text{ G}\Omega$ .

$$C_{diff} = \epsilon \epsilon_0 K = \sqrt{\frac{Az^2ze^2\epsilon\epsilon_0C_iN_A}{kT}}$$

where  $z$  is the ion valence number,  $A$  is a constant,  $e$  the charge of an electron equal to  $1.6 \times 10^{-19}$ ,  $N_A$  is Avogadro's number,  $C_i$  is the concentration of the ionic solution (mol/l),  $\epsilon\epsilon_0$  is

the absolute dielectric constant of the sample,  $T$  is the absolute temperature, and  $k$  is the Boltzmann constant.

Another parasitic impedance component, as shown in Fig. 5b, is the faradaic resistance or the electron transfer resistance ( $R_t$ ), which is in parallel with the double layer capacitance. Electron transfer resistance results from tunneling of electrons from the conductive electrodes into the bulk electrolyte and to and through the DNA molecules. The last remaining parasitic component of the circuit model is the bulk solution resistance ( $R_s$ ). As shown in Fig. 5b, it is in series with the above two components and results from the resistivity of the electrolyte.

We can determine the percentage contribution of each component and its effect on the measured impedance results at 15 KHz, by finding their value at this frequency and possibly simplify our circuit model. Starting with the top branch of the circuit model and considering the fact that both  $R_t$  and  $R_s$  are frequency-independent, and by looking at the total measured impedance at 1Hz, equal to  $0.5 \text{ G}\Omega$ , we can estimate that  $R_t$  in series with  $R_p$  can be no less than  $0.5 \text{ G}\Omega$  across the whole frequency spectrum. At the beginning of this section, we also estimated that the value of double layer capacitance at 15 kHz is about  $\sim 1 \text{ G}\Omega$ . This means that the equivalent impedance of  $C_{dl}$  and  $R_t$  in parallel with each other and in series with  $R_s$  must also be greater than  $0.5 \text{ G}\Omega$ . Comparing this value to the total measured impedance of the sensors at 15kHz, which is  $3.6 \text{ M}\Omega$ , we are able to assume that the top branch, containing  $C_{dl}$ ,  $R_t$ , and  $R_s$ , is essentially an open circuit at this frequency and only two parallel components of  $C_f$  and  $R_f$  are affecting imaginary and real components of measured impedance respectively. Assuming that, we are then able to categorize three main physical mechanisms affecting both out-of-phase (imaginary) and in-phase (real) parts of the measured impedance. The dominant phenomenon, which mainly affects imaginary components of the measured impedance, is an increase in relative dielectric permittivity ( $\kappa\epsilon_{sol}$ ) of the solution at the nanopip sensors interface due to formation of the double-stranded helix, which results in an increase in capacitance and thus a decrease in measured impedance.

$$C_f = \frac{\kappa\epsilon_{sol}\epsilon_0}{K};$$

where  $\kappa\epsilon_{sol}$  is the relative dielectric permittivity of the solution and  $K$  is a geometrical factor of the electrode structures.

AC coupling is the second dominant mechanism affecting change in both real and imaginary components of the measured impedance. The relative dielectric permittivity of the solution ( $\kappa\epsilon_{sol}$ ) is explicitly affected by the DNA dipole moment (dependent upon both DNA length and charge) and concentration of the DNA molecules in the solution. The DNA counter ions, free as well as condensed, contribute to the oscillating polarization in the applied electric field and thus determine the dielectric response of the DNA solution. In the presence of an AC field, polarization is inducing and a flow of net charge resulting from the DNA counter ions occurs. There are mobile charges in and around the DNA molecules forming a shield of ions around the backbone; which results in the formation of a dipole in the DNA when we



electrically probed in solution (Esfandyarpour et al. 2013). The third and least significant cause of the impedance change, mainly the real component, is the modulation of the faradaic or tunneling current across the nanotip sensors' conductive electrodes due to the formation of the double-stranded helix at the sensor interface, which creates new paths for electrons to tunnel and pass through the DNA molecules, and affects on out-of-phase response of the sensors.

### 3.3 Control experiments

In order to demonstrate the sensitivity and specificity of our nanotip sensors, detection of single point mutations, and the accuracy of observed impedance change, three sets of control experiments were performed as follows.

**3.3.1 Electrical control experiments**—Two electrical control experiments were performed using non-complementary and single-base mismatched single stranded DNA molecules, with the concentration of 10  $\mu$ M. As shown in Fig. 3e, when the complementary single-stranded target DNA was replaced by single stranded non-complementary DNA, negligible impedance change ( $\sim 1\%$ ) was observed. It indicates, as expected, no double-stranded helix is formed between a pair of non-complementary sequences at the sensor interface and as a result a negligible impedance change is observed. To evaluate the selective detection of single point mutations, the mutated target oligonucleotides were designed with a single-base mismatch at 27th position. As shown in Fig. 3d, the hybridization occurring between the immobilized single stranded probe DNA and the single-base mismatched target DNA generated about  $\sim 9$  kohm change in measured impedance value. It represents a reduction of about 89% with respect to the signal generated by complementary single stranded DNA molecules with the same concentration (10 pM), thus showing a highly selective response of the nanotip sensors. The results suggest that nanotip sensors are applicable for detecting single base differences, allowing precise discrimination between fully complementary and mismatched sequences. These control experiments verify that the typical change in impedance is unique to the fully complementary target DNA, as indicated above (Tables 1 and 2).

**3.3.2 Optical verification**—To demonstrate the selectivity and the specificity of probe to target hybridization and single point mutation detection, we performed optical verification. For this study, fluorescently labeled complementary and single mismatch DNA, both at the concentration of 10  $\mu$ M, were exposed to the nanotip sensors coated with the primary single-stranded DNA molecules. After performing wash steps for both nanotip sensors, one treated with fluorescently labeled complimentary DNA and the other with fluorescently labeled single mismatch DNA, we examined the sensors using an epi-fluorescence microscope. As expected, strong fluorescent signals were obtained from the nanotip sensor treated with complementary target DNA, where the bright sensor tip is clearly visible in Fig. 4b. On the contrary, very weak fluorescent signals were obtained from the nanotip sensor treated with single mismatch DNA molecules, and the sensor tip is hardly visible in Fig. 4a. Fluorescence intensity analysis, shown in Fig. 4c and Table 3, shows an order of magnitude less fluorescence intensity level for the single mismatch DNA experiment compared to the complementary DNA, reflecting the expected difference in hybridization efficiency. These

results confirm the specificity of binding between the complimentary single stranded DNA molecules and single stranded probe DNA molecules as well as the nanotip sensor's utility in detecting single point mutations.

### 3.4 Quantitative measurements and reproducibility

To investigate the detection limit and the capacity of the nanotip sensors for quantitative measurements, we tested their performance on different concentrations of complementary single stranded DNA ranging from 10  $\mu$ M to 10pM. Each experiment was repeated at least three times. Through these results, we derived a calibration curve of the nanotip sensors displaying a concentration-dependent change in electrical impedance (Fig. 5a), As depicted in Fig. 5a and Fig. 3f, 10  $\mu$ M complementary single-stranded DNA concentration results in an impedance change of about ~26 %, 10 nM results in ~14 % change, and 10pM in about ~8 % change, while there was only a change of ~1 % for non-complementary single stranded DNA with the concentration of 10  $\mu$ M.

## 4 Conclusion

Here we presented a novel nanotip sensor design and demonstrated its effectiveness and sensitivity at sequence-specific detection of DNA oligonucleotides. We observed during the design that the detection limit could be improved by using a thickness controllable thin film layer (~ 20 nm) as the sensing layer. We designed the nanotip sensors in 3D to improve the bio-species hit rate and speed of detection. Their amenability to an array design allows scalability up to hundreds of thousands sensors in a single device, enabling high-throughput genomics studies. Our current design is fabricated on a four-inch silicon wafer, with a density of 5000 sensors/cm<sup>2</sup>. The array is fabricated through well-established photolithography processes coupled with a focused ion beam etching process, which makes it a high throughput platform well suited to mass production. The results we present here demonstrate the utility of our impedance-based nanotip sensors for rapid, inexpensive, high throughput, real-time, and label-free sequence specific detection of oligonucleotides, including precise discrimination against mismatched oligonucleotides. We also studied the concentration dependency of nanotip sensors, which indicated the utility of the sensors for detecting double-stranded helix formation in a target sample as low as 10 pM. Our novel design therefore offers an attractive, label-free, real-time alternative to the traditional genosensor arrays. Since the sensor has a rigid nano-structure, further developments of this technology could ultimately be used for gene expression measurements within a single living cell. We anticipate that our nanotip sensors can be leveraged to develop a novel class of electronic DNA nanobiosensors that could greatly improve the feasibility of clinical genetic diagnostics.

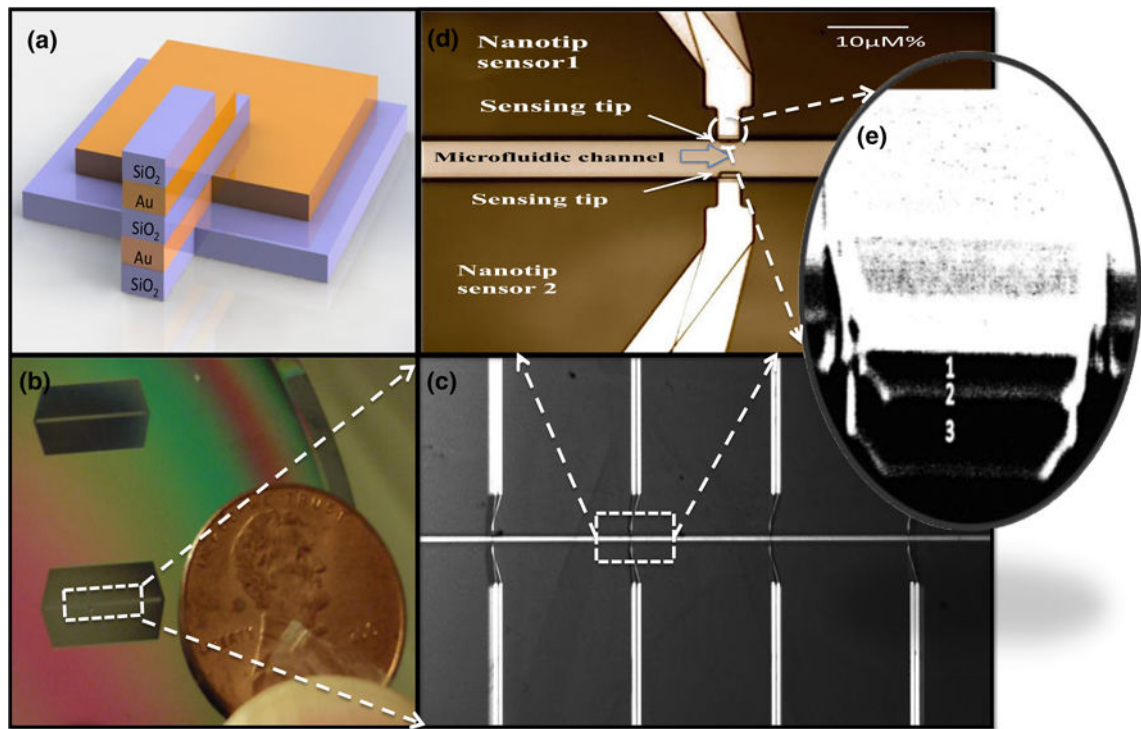
## Acknowledgments

The authors like to thank Weihong Xu, Bob St. Onge, Richard W. Hyman and Raeka Aiyar for useful comments and discussions. This work was supported by the National Institutes of Health Grant No. P01HG000205.

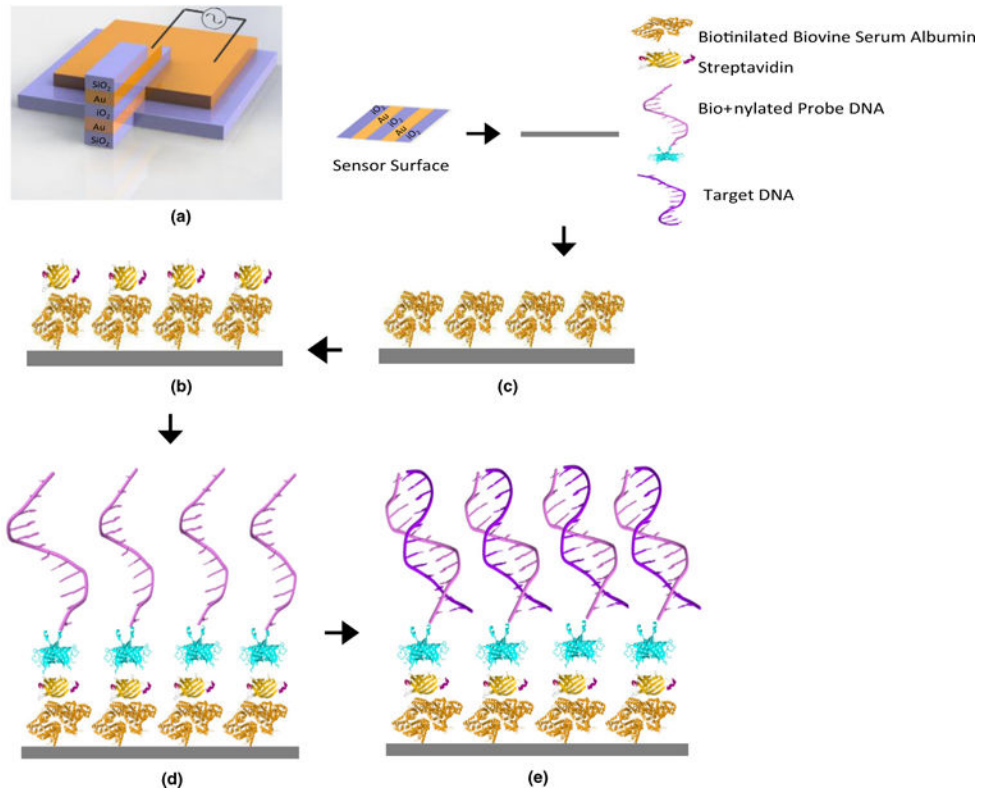
## References

- Adams MD, et al. Complementary DNA sequencing: expressed sequence tags and human genome project. *Science*. 1991; 252(5013):1651–1656. [PubMed: 2047873]
- Ahmadian A, et al. Single-nucleotide polymorphism analysis by pyrosequencing. *Anal Biochem*. 2000; 280(1):103–110. [PubMed: 10805527]
- Ansoorge W, et al. Automated DNA sequencing: ultrasensitive detection of fluorescent bands during electrophoresis. *Nucleic Acids Research*. 1987; 15(11):4593–4602. [PubMed: 3588303]
- Cui Y, et al. Nanowire Nanosensors for highly sensitive and selective detection of biological and chemical species. *Science*. 2001; 293(5533):1289–1292. [PubMed: 11509722]
- Drumm ML, Konstan MW, Schluchter MD, Handler A, Pace R, Zou F, Zariwala M, Fargo D, Xu AR, Dunn JM, Darrah RJ, Dorfman R, Sandford AJ, Corey M, Zielenski J, Durie P, Goddard K, Yankaskas JR, Wright FA, Knowles MR, Modifier G. *Gene Study*. *N Engl J Med*. 2005; 353:1443. [PubMed: 16207846]
- Esfandyarpour R, et al. Microneedle biosensor: A method for direct label-free real time protein detection. *Sensors and Actuators B: Chemical*. 2013; 177:848–855.
- Gao Z, et al. Silicon nanowire arrays for label-free detection of DNA. *Anal Chem*. 2007; 79(9):3291–3297. [PubMed: 17407259]
- Hashemi Rafsanjani SM, Cheng T, Mittler S, Rangan C. Theoretical proposal for a biosensing approach based on a linear array of immobilized gold nanoparticles. *J Appl Phys*. 2010; 107:094303.
- Huse SM, et al. Accuracy and quality of massively parallel DNA pyrosequencing. *Genome Biol*. 2007; 8(7):R143. [PubMed: 17659080]
- Kannan B, et al. High-sensitivity, label-free DNA sensors using electrochemically active conducting polymers. *Anal Chem*. 2011; 83(9):3415–3421. [PubMed: 21466209]
- Kricka LJ. Stains, labels and detection strategies for nucleic acids as-says. *Annals of Clinical Biochemistry*. 2002; 39(2):114–129. [PubMed: 11928759]
- Li Z, et al. Sequence-Specific label-Free DNA Sensors Based on Silicon Nanowires. *Nano Letters*. 2004; 4(2):245–247.
- Li Z, et al. Silicon nanowires for sequence-specific DNA sensing: device fabrication and simulation. *Applied Physics A*. 2005; 80(6):1257–1263.
- McBride LJ, et al. Automated DNA sequencing methods involving polymerase chain reaction. *Clin Chem*. 1989; 35(11):2196–2201. [PubMed: 2582616]
- Metzker ML. Emerging technologies in DNA sequencing. *Genome Research*. 2005; 15(12):1767–1776. [PubMed: 16339375]
- Metzker ML, Lu J, Gibbs RA. Electrophoretically uniform fluorescent dyes for automated DNA sequencing. *Science*. 1996; 271(5254):1420–1422. [PubMed: 8596915]
- Park SJ, Taton TA, Mirkin CA. Array-based electrical detection of DNA with Nanoparticle probes. *Science*. 2002; 295(5559):1503–1506. [PubMed: 11859188]
- Quince C, et al. Accurate determination of microbial diversity from 454 pyrosequencing data. *Nat Methods*. 2009a; 6(9):639–641. [PubMed: 19668203]
- Quince C, et al. Accurate determination of microbial diversity from 454 pyrosequencing data. *Nat Methods*. 2009b; 6(9):639–641. [PubMed: 19668203]
- Ronaghi M, et al. Real-time DNA sequencing using detection of pyrophosphate release. *Anal Biochem*. 1996; 242(1):84–89. [PubMed: 8923969]
- Ronaghi M. Pyrosequencing sheds light on DNA sequencing. *Genome Res*. 2001; 11(1):3–11. [PubMed: 11156611]
- Ronaghi M, Uhlén M, Nyrén P. A sequencing method based on real-time pyrophosphate. *Science*. 1998; 281(5375):363–365. [PubMed: 9705713]
- Roses MD, Allen D. Apolipoprotein E alleles as risk factors in Alzheimer's disease. *Annu Rev Med*. 1996; 47(1):387–400. [PubMed: 8712790]
- Sanger F, et al. The nucleotide sequence of bacteriophage  $\phi$ X174. *J Mol Biol*. 1978; 125(2):225–246. [PubMed: 731693]

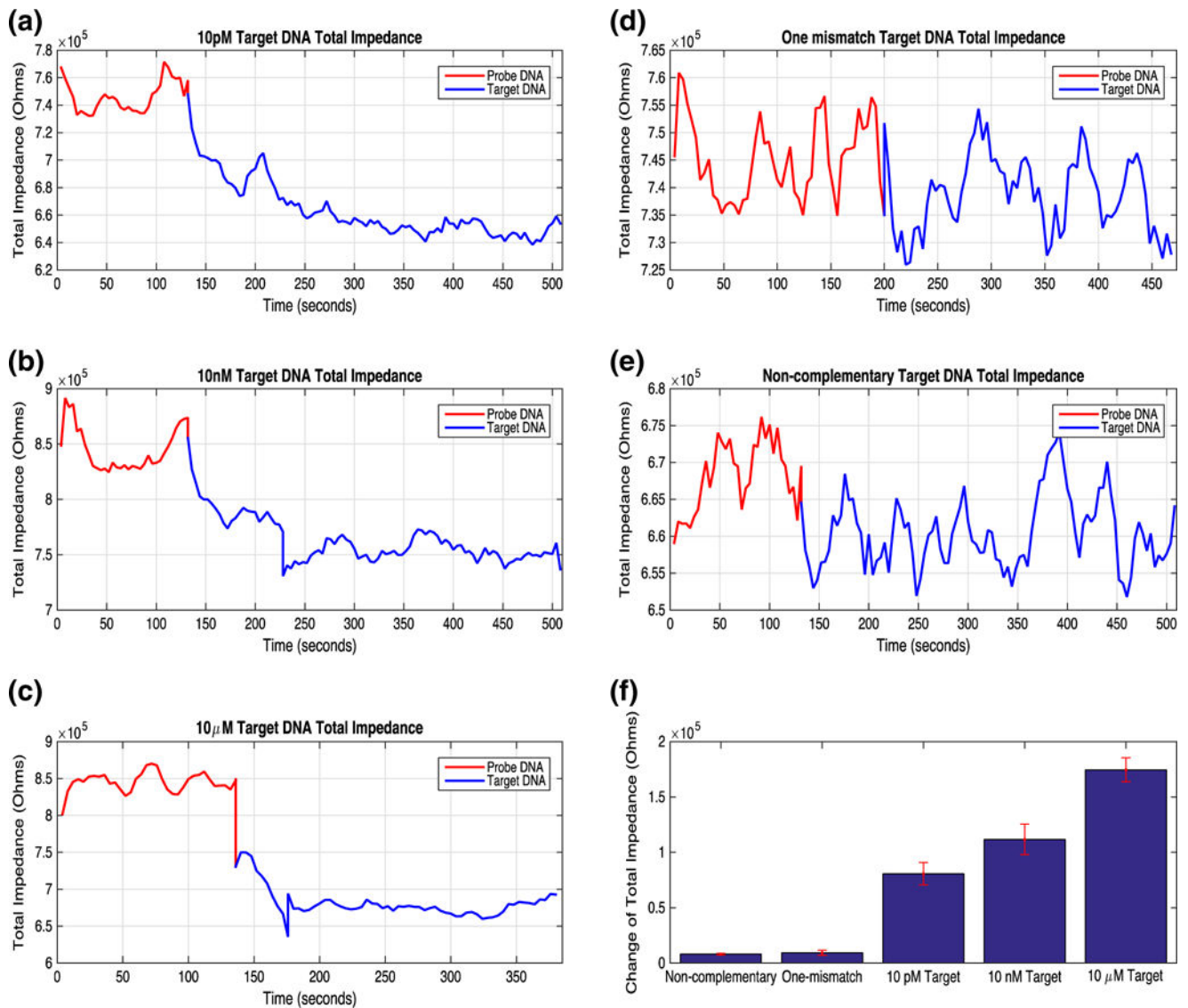
- Sanger F, Nicklen S, Coulson AR. DNA sequencing with chain-terminating inhibitors. *Proc Natl Acad Sci.* 1977; 74(12):5463–5467. [PubMed: 271968]
- Smith LM, et al. Fluorescence detection in automated DNA sequence analysis. *Nature.* 1986; 321:674–679. [PubMed: 3713851]
- Velculescu VE, et al. Serial analysis of gene expression. *Science.* 1995; 270(5235):484–487. [PubMed: 7570003]
- Wang J, et al. Peptide nucleic acid probes for sequence-specific DNA biosensors. *J Am Chem Soc.* 1996; 118(33):7667–7670.
- Xie P, et al. Local electrical potential detection of DNA by nanowire-nanopore sensors. *Nat Nanotechnol.* 2012; 7(2):119–125. [PubMed: 22157724]
- Zhang N, Apella DH. Advantages of peptide nucleic acids as diagnostic platforms for detection of nucleic acids in resource-limited settings. *Journal of Infectious Diseases.* 2010; 201(Supplement 1):S42–S45. [PubMed: 20225945]
- Zhang GJ, et al. Highly sensitive measurements of PNA-DNA hybridization using oxide-etched silicon Nanowire biosensors. *Biosensors and Bioelectronics.* 2008; 23(11):1701–1707. [PubMed: 18356037]



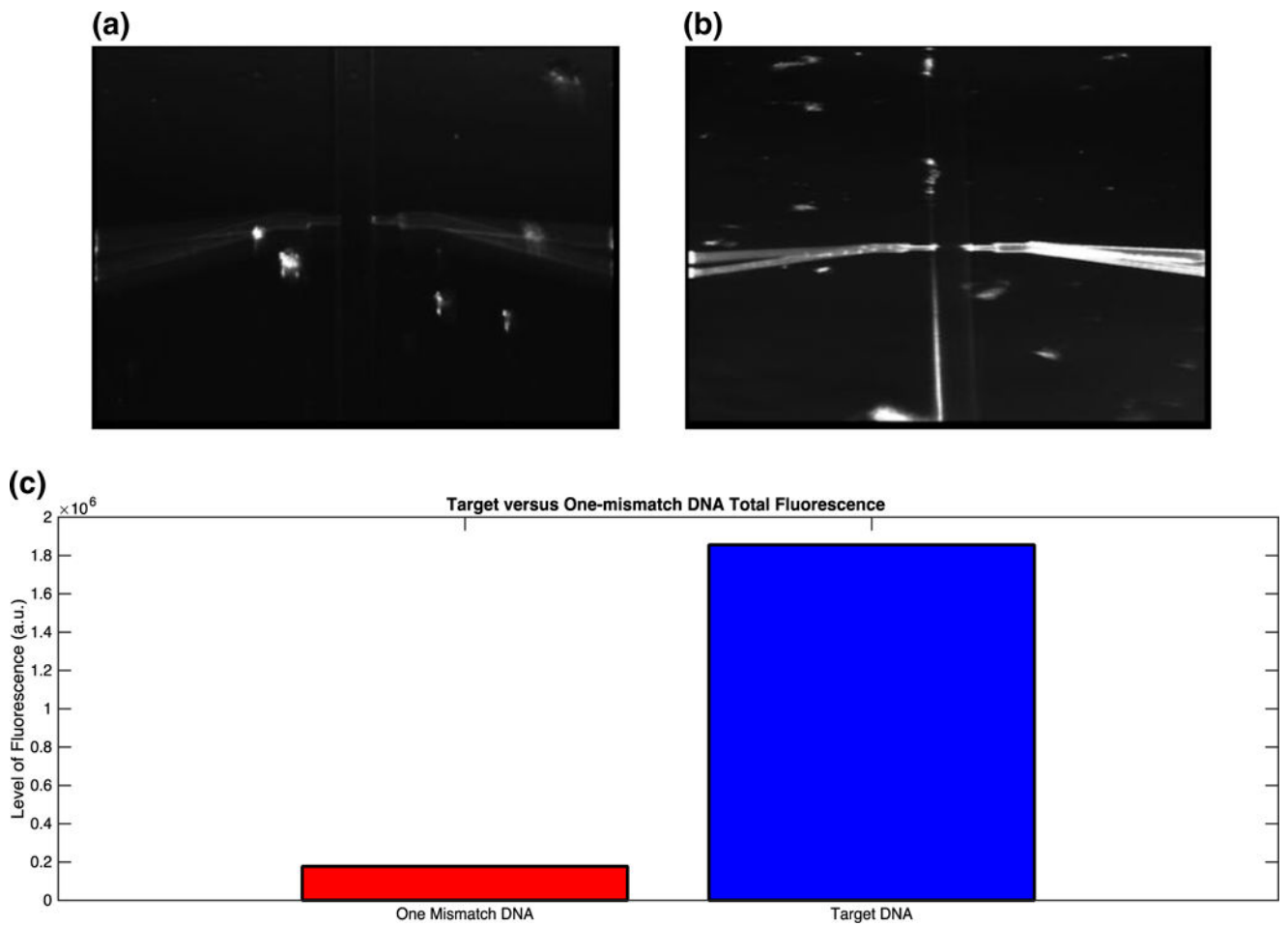
**Fig. 1.**  
**a** Schematic of a single nanotip sensor three-dimensional (not to scale) **b** Optical micrograph of nanotip sensors compare to a US penny size **c** Optical micrograph of nanotip sensors **d** Top view optical micrograph of two nanotip sensors in a microfluidic channel **e** SEM image of a single nanotip sensor, where 1 and 3 are conductive layers and 2 is the middle oxide sensitive layer



**Fig. 2.** Schematic illustration of surface modification processes, showing probes DNA immobilization and probe-target DNA hybridization on nanotip sensors surface

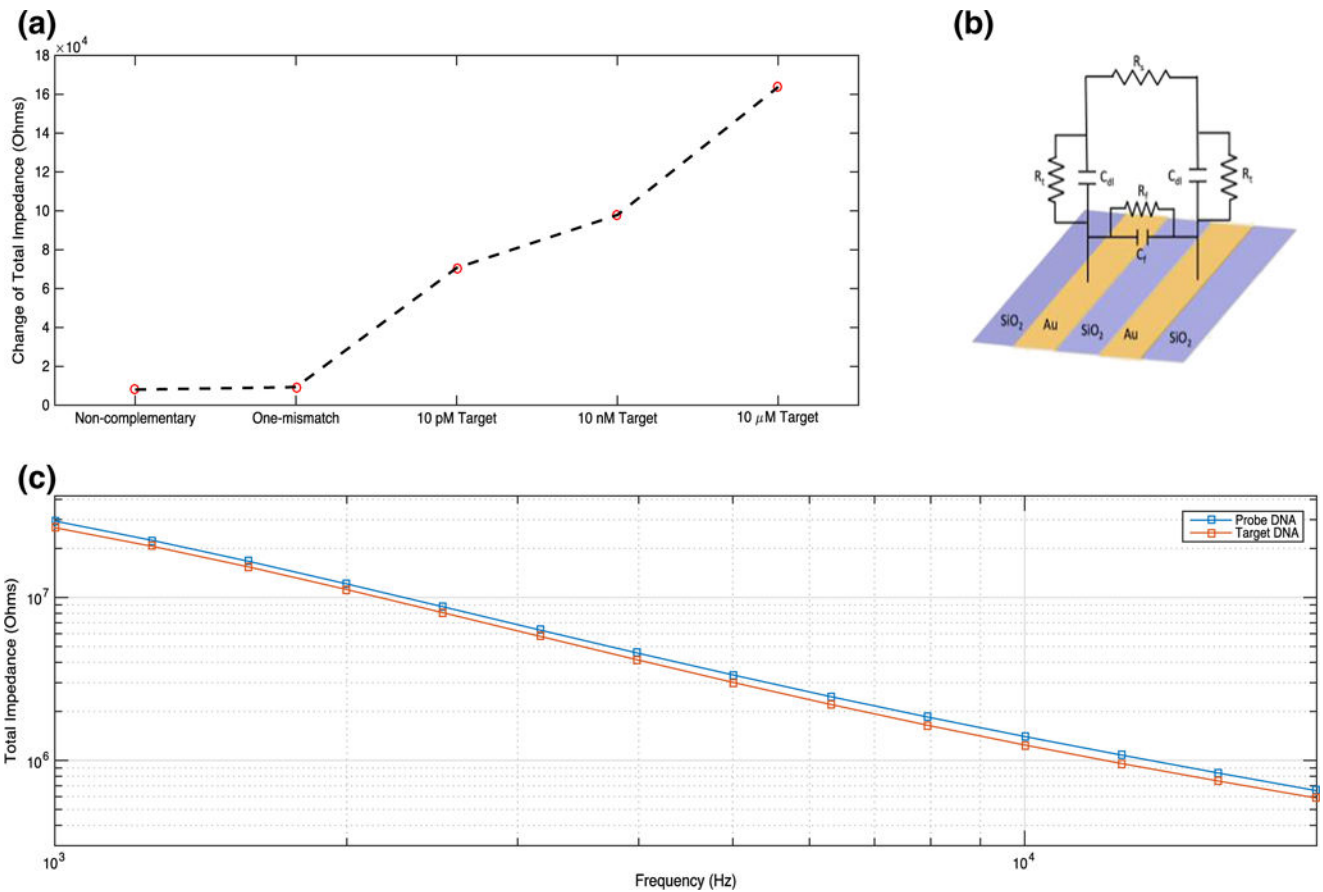


**Fig. 3.** Measured nanotip sensors' impedance change for variety of target complementary single stranded DNA concentrations **a** 10pM, **b** 10 nM, **c** 10  $\mu$ M and for **d** 10  $\mu$ M single-base mismatched DNA (control) **e** 10  $\mu$ M non-complementary DNA (control). **f** Comparison of measured impedance difference at 15 KHz for various concentrations of sequence specific complementary, non-complementary and single-base mismatched DNA



**Fig. 4.** **a** Fluorescent images of nanotip sensor treated with 10  $\mu$ M fluorescently labeled one-mismatch DNA **b** Fluorescent images of nanotip sensor treated with 10  $\mu$ M fluorescently labeled complementary DNA, both after wash. **c** Comparison of the fluorescence intensity signals for single-mismatch and complimentary DNA



**Fig. 5.**

**a** Experimentally obtained calibration curve of nanotip sensors for target oligonucleotide at room temperature (23 °C) **b** Circuit model at the interface of a nanotip sensor with the electrolyte showing existing parasitic components such as fringing capacitance ( $C_f$ ), resistance across the double layer at the sensor tip between the electrodes ( $R_f$ ), double layer capacitance on each electrode surface ( $C_{dl}$ ), electron transfer parasitic resistance from the electrodes into the bulk solution ( $R_t$ ) and the bulk resistance of the electrolyte ( $R_s$ ) **c** Impedance spectra of functionalized nanotip sensors before and after complementary DNA hybridization

**Table 1**

List of the oligonucleotides used in impedance detections. The target DNA is complementary to the probe DNA. One-mismatch DNA has one base mismatch at the 27th position (bold letter in the table) starting from 5' end. The non-complementary DNA has mismatch bases at all positions

Name	Sequence	Length (ss)
Probe DNA	5'-Biotin-ACACCTGCACTACCACACTCCCTCACACTGACAAATGATCACCCC-3'	45
Target DNA	5'-AGGTGTGGGGTGATCATTGTCAGTGTGAGGGAGTGTGGTAGTGC-3'	45
One-mismatch DNA	5'-AGGTGTGGGGTGATCATTGTCAGTGC <b>G</b> AGGGAGTGTGGTAGTGC-3'	45
Non-complementary DNA	5'-CTTGTGTTTTGTCGACGGGTGACTCACACTTTCTGTGTGCTGTA-3'	45

Author Manuscript

Author Manuscript

Author Manuscript

Author Manuscript

**Table 2**

Z comparison of the total, real and imaginary components of measured impedance levels, for non-complementary, single-mismatch, and complementary target DNA samples. The average value of the signals was used to calculate the change values

	$ Z $ (ohms)	$Z_{re}$ (ohms)	$Z_{im}$ (ohms)	Percentage of Change (%)
Non-complementary DNA (10 $\mu$ M)	7997	16,941	9252	~1
Single-mismatch DNA (10 $\mu$ M)	9309	3979	9721	~1
10 pM Target DNA	80,674	35,885	92,947	~8
10 nM Target DNA	111,670	97,797	112,400	~14
10 $\mu$ M Target DNA	174,600	135,260	177,730	~26

**Table 3**

Fluorescence intensity level analysis for complimentary and single control mismatch experiments, which quantified surface absorptions of complimentary and single-mismatch DNA samples on the sensors. Quantifications were performed using ImageJ on the regions of both sensor and background. The corrected total sensor fluorescence (CTSF) was calculated (CTSF = Integrated Density of Sensor Area – Area of Selected Sensor × Mean Fluorescence of Background)

	Area	Mean Fluorescence	Integrated Density	CTSF
Single-mismatch DNA	23,947	14.534	348,037	177,582
Single-mismatch background	380	7.118	2705	–
Target DNA	21,608	135.952	2,937,654	1,855,698
Target background	349	50.072	17,475	–